Journal of
Computational and Theoretical Nanoscience
Vol. 2, 251–255, 2005

Nanotube Bending Due to Central Loading

Kausala Mylvaganam and L. C. Zhang*

School of Aerospace, Mechanical and Mechatronic Engineering, The University of Sydney, NSW 2006, Australia

RESEARCH ARTICLE

This paper investigates the behaviour of carbon nanotubes under central loading by diamond indentors. Molecular dynamics simulations were performed on short and long carbon nanotubes of various radii using spherical diamond indentors for loading. It was found that the zigzag tube fails after it reaches a bending angle of 62° and a global strain of 14.5% irrespective of the tube radii, that the maximum load the tube can endure increases with the tube radius but is independent of the tube length, and that the deformation capacity of a carbon nanotube (CNT) varies with the type of loading.

Keywords: Carbon Nanotube, Diamond Indentor, Molecular Dynamics, Indentation.

1. INTRODUCTION

Single-walled and multi-walled nanotubes undergoing axial tension,[1,2] compression,[3,4] bending[5,6] and twisting[7] have been studied to a certain extent. Techniques for reliable molecular dynamics simulations have also been investigated comprehensively.[2] Both simulations and experiments have shown that single-walled nanotubes (SWNTs) can withstand 10–40% deformation before they break. Simulations also show that nanotubes under substantial deformation can still remain elastic. As such carbon nanotube-based composites are expected to be extraordinarily strong, of light-weight and of high wear resistance under the sliding and indentation of hard asperities.[8] To realize these, however, one first needs to know more about the behaviour of CNTs under complex mechanical loading.

Moreover, CNTs are being used as actual components in a number of prototype devices such as rectifiers, nanoswitches, etc. For this, the positioning of a nanotube can be attained via manipulation with a scanning probe tip.[9] This procedure is likely to introduce a large mechanical deformation on the CNT. Shen and Jiang[10] performed a nanoindentation on the top of a tube using a scanning probe microscope with a diamond tip and investigated the radial compression of multiwalled carbon nanotubes under an asymmetric stress. They found that the radial compression varied nonlinearly with the applied stress and estimated the compressive strength to be well beyond 5.3 GPa. Tombler et al.[11] have reported the electromechanical characteristics of individual SWNTs when deformed by an AFM tip. In their experiment, they positioned the AFM tip above the centre of an SWNT suspended over trenches fabricated on a SiO_2 surface. Then they measured the deflection and the resistance of the suspended CNT on pushing and retracting many times as a function of time. They found that the force versus nanotube deflection curve right after the tube-tip contact was cubic, that the mechanical deformation was highly reversible and that the conductance was reduced by two orders of magnitude. However, a theoretical foundation is unavailable.

This study focuses theoretically on a similar mechanical testing configuration to that of Tombler et al.'s experiment. The nanotube deformation under a diamond indentor will be investigated by molecular dynamics method. Both short and long zigzag nanotubes of various radii will be studied.

2. COMPUTATIONAL TECHNIQUES

The inter-atomic interactions of the classical molecular-dynamics method were described by reactive bond-order hydrocarbon potential formulated by Brenner.[12,13] This potential allows for bond formation and breaking to occur and has been successfully used to simulate the deformation of CNTs,[2] and the indentation of diamond and grapheme surfaces with CNT tips.[14] The indentor-nanotube interactions were described by a two-body Morse potential, $V(r_{ij}) = D[e^{-2\alpha(r_{ij}-r_0)} - 2e^{-\alpha(r_{ij}-r_0)}]$, which has been successfully used for a large number of

*Author to whom correspondence should be addressed.

1546-198X/2005/2/251/005 doi:10.1166/jctn.2005.108

machining and indentation processes involving substrate-tool interactions.[15–17] The parameters used in the Morse potential are, $\alpha = 5.110$ Å^{-1}, $D = 139.71$ kcal mol^{-1}, and $r_0 = 2.522$ Å.

Open single-walled zigzag nanotubes (9,0), (17,0) and (34,0) of various radii (R) having lengths of ~75 Å and ~246 Å were loaded at the centre with spherical diamond indentors of radii 5.35 Å and 21.4 Å, respectively. In all the simulations, two rings of atoms at both ends of the nanotube were clamped and the indentor was placed in the middle at 5 Å above the surface of the nanotube. As pointed out in our earlier work[2] on nanotubes, in order to minimize the heat conduction problem and improve the computational efficiency, Berendsen thermostat was applied to all atoms except the two rings of atoms that were rigidly held. The simulations were carried out at 300 K with a time step of 0.5 fs. The indentor was moved towards the nanotube in increments of 0.001 Å. The loading continued until the tube failed. The force on the indentor were calculated at each 0.5 Å of its displacement steps and plotted against the average deflection, δ, of the nanotube. The tube was unloaded at different stages of loading to examine its response to mechanical unloading at different loading levels.

To understand the mechanism difference of a CNT under different bending deformation, the pure bending of the CNT was also investigated. In this case, 10 rows of atoms on each end of the (17,0) CNT were rotated out of plane in steps of 2 degrees. First, these atoms were held rigid at their rotated positions and the rest were relaxed to a minimum energy using the conjugate gradient algorithm. Then those relaxed atoms were held at their new positions and the end atoms that were held rigid in the previous step were relaxed to the minimum energy. This procedure was repeated up to a bending angle of 64 degrees.

3. RESULTS AND DISCUSSION

As the indentor is pushed against the surface of the nanotube, flattening and bending developed on the tube and subsequently the tube failed at its ends. This deformation mechanism is analyzed and the variation with tube parameters and indentor size are compared in the following sections.

3.1. Central Loading by a Small Indentor (Radius = 5.35 Å)

3.1.1. Short (9,0), (17,0) and (34,0) Nanotubes (Length = 75.3 Å)

During the loading process, once the indentor moved down by ~3.0 Å, the tube wall that was close to the indentor experienced compression. The tube started to flatten right below the indentor. As loading continued, the top surface of the tube was pushed in more and more beneath the indentor; along the tube the circular cross-section became

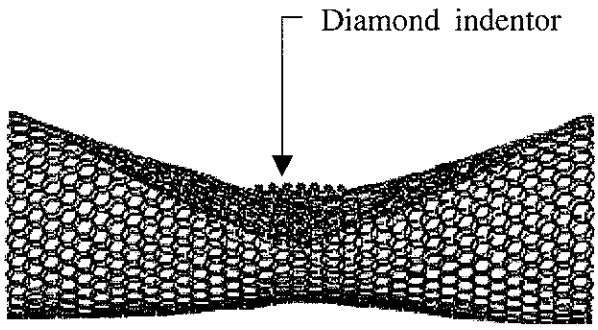

Fig. 1. Side view of a (34,0) zigzag tube showing the inward bending due to the flattening of the opposite wall on moving the indentor by 20.0 Å.

elliptic with a flattened top surface. On further loading, the opposite wall became flattened and as a result it appeared as if the tube bend inwards as shown in Figure 1. This shows that the stress is released in the transverse direction. Then the tube started to bend and cross-section ovalisation and flattening progressed in the longitudinal direction as shown in Figure 2. The distance between the opposite walls of the tube beneath the indentor became as small as 2 Å. Further loading caused structural damage to the tube and finally the tube was broken at both ends. Figure 3(a)–(c) shows the side view of the three different radii tubes studied here, under maximum loading. Unloading from any

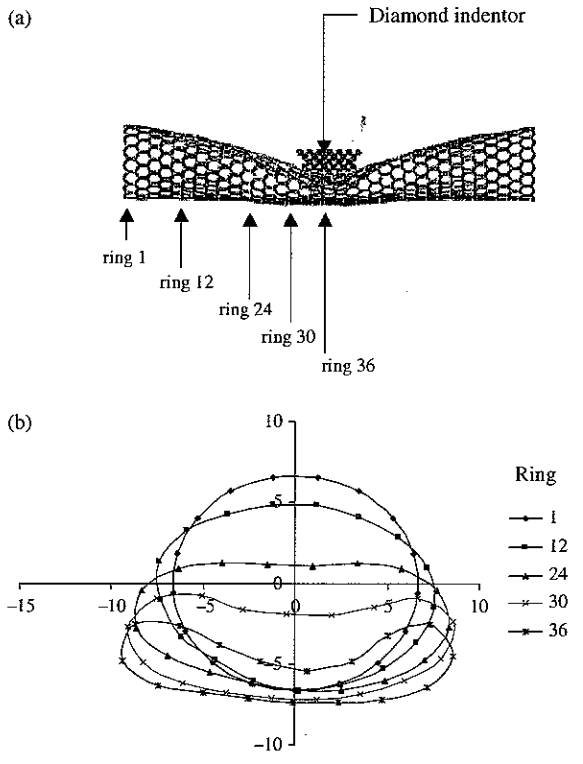

Fig. 2. (a) (17,0) CNT showing the ring positions addressed in Figure 2(b) during loading (the indentor was moved by 15 Å) (b) Cross-section ovalisation, flattening and compression of the (17,0) CNT during loading (the indentor was moved by 15 Å).

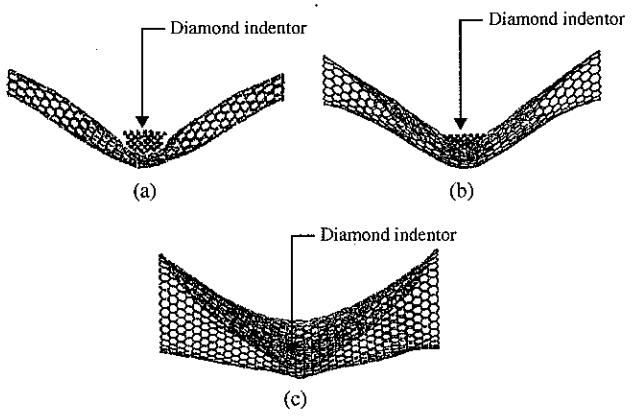

Fig. 3. Side view of a (a) (9,0), (b) (17,0) and (c) (34,0) CNTs under maximum loading with an indentor.

step before the structural damage showed that the deformation was fully elastic. The above changes observed at different indentor positions for tubes with various radii are summarized in Table I.

The Force-Deflection curves of the three tubes studied here follow a cubic relation as shown in Figure 4, which confirms that the experimental findings by Tombler et al.[11] was theoretically reasonable. The result also shows that the maximum force which the tube can withstand increases with its diameter. Assuming that the deflected SWNT forms a triangle with its original configuration, the global strain, ε, distributed over the length of the CNT can be approximated to $[(4\delta^2+l^2)^{1/2}-l]/l$, where δ is the deflection and l is the length of the tube as in Ref. [11]. Accordingly, the maximum global strain of the tube is calculated as 14.5% and this is independent of the tube radii as the average maximum deflection, δ, is nearly the same for a given length of tubes with various radii.

It is also interesting to see how the above bending differs from pure bending. Figure 5 compares the deformation patterns of some selected atomic rings along the tube axis when the tube was bent by indentation and pure bending

Table I. The changes observed during centre loading for tubes with a length of 75.3 Å.

Changes observed	(9,0) $R = 3.523$ Å	(17,0) $R = 6.655$ Å	(34,0) $R = 13.301$ Å
Distance by which the indentor moved to begin deformation	~3 Å	~3 Å	~3 Å
Distance by which the indentor moved for structural deformation	~27 Å	~30 Å	~36 Å
Distance by which the indentor moved at ultimate failure	29.0 Å	32.0 Å	40.5 Å
Average maximum deflection (δ)	~23 Å	~23 Å	~24 Å
Maximum force on tool (nN)	77.8	154.0	231.0
Maximum bending angle	~62°	~62°	~64°

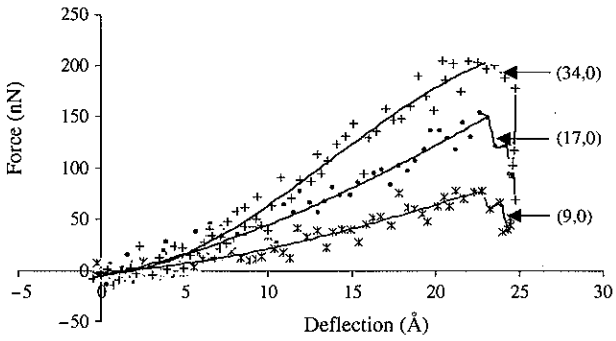

Fig. 4. Force-deflection curves of CNTs of different radii on loading with an indentor.

to nearly the same angle. It is clear that with the indentor, the tube is pushed in at the centre and the ovalisation of the tube near the end is more pronounced compared to pure bending. Furthermore, in the former, since the ends of the tube were hold rigidly, the whole tube is under

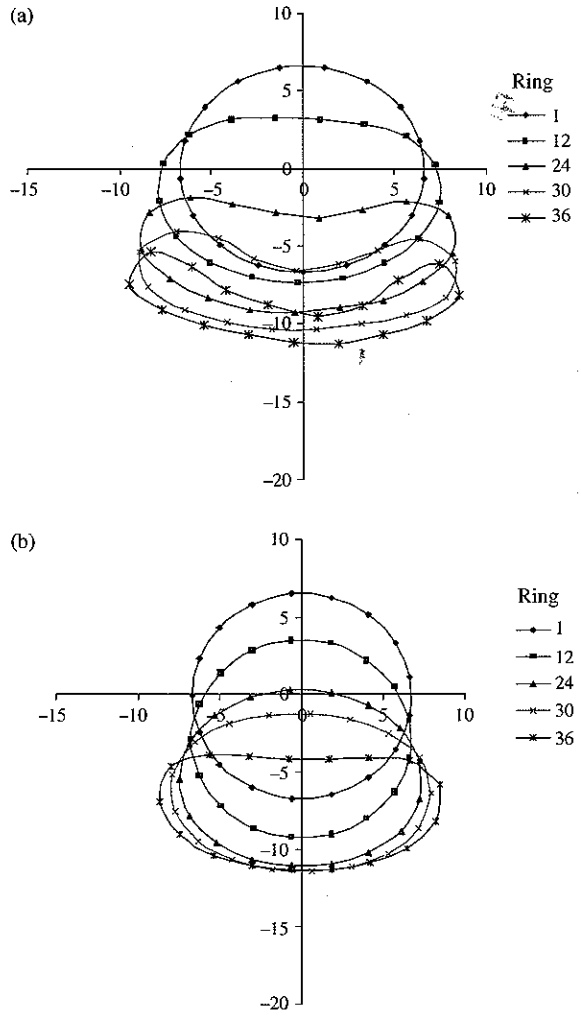

Fig. 5. Comparison of cross-sectional changes of a (17,0) CNT when the bending angle was ~30° (a) on centre loading (b) on pure bending (for ring labeling see Fig. 2(a)).

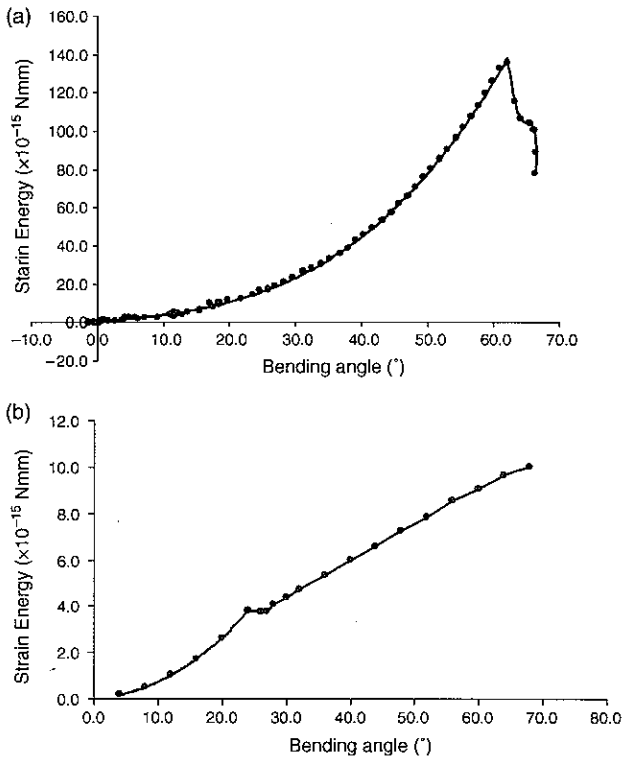

Fig. 6. Variation of strain energy with bending angle (a) under centre loading (b) in pure bending of a (17,0) CNT.

tensile stress longitudinally when the tube's overall deflection is sufficiently large. The strain energy, which is calculated as the difference in total energy during loading and before loading, varies cubically with the bending angle as shown in Figure 6(a). In pure bending, however, the inner wall of the tube experiences a compressive stress while the outer wall experiences a continuous tension and therefore forms a local kinking as shown in Figure 7. Here initially the strain energy varies cubically with the bending angle then at the onset of kinking it drops a little and thereafter it varies linearly as shown in Figure 6(b). A comparision of the magnitude of the strain energy values shows that after kinking the tube is less strained under pure bending compared to central loading; for example, at a bending angle of 56° the strain energy values are 8.5×10^{-15} and 1.1×10^{-13} Nmm, respectively.

It is interesting to highlight here that the local buckling and overlisation pattern of the CNT under pure bending is very similar to that of a continuum metal tube when its l/R is greater than 10 and R/t (t is the thickness) is less than 75,[18, 19] although the CNT wall is not

Fig. 7. Pure bending of a (17,0) CNT showing the kink at a bending angle of 56°.

a continuum. This observation seems to further support the rationale of characterization of the equivalent mechanical properties of CNTs under the continuum mechanics umbrella.[6, 20]

3.1.2. A Long (17,0) Nanotube (Length = 245.8 Å)

Initially, the tube got flattened beneath the indentor on loading and started to bend as in the case of a short nanotube. At the early stages, apart from the little flattening beneath the indentor, the tube ovalisation is not prominent. As the loading continued, flattening increased, the distance between the opposite walls decreased to ~3 Å and the cross-sectional deformation became asymmetric. Since a long tube is much flexible both axially and transversely compared with a short tube, it swung side way as a result of the asymmetric loading of the indentor. Thus, on further loading, i.e, when the indentor moved by 54.5 Å, the indentor was no longer on the tube and the tube became free from external loading. As a result, the tube returned to its initial configuration. However, the indentation results indicate that unlike a short tube, the indentor needs to move a long distance to make it fail.

3.2. Central Loading of a Long (17,0) and (34,0) Nanotubes (Length = 245.8 Å) by a Large Indentor (Radius = 21.4 Å)

Initial flattening of the tube occurs once the indentor moved by ~3 Å. As loading continued, unlike the loading with the small indentor, initially the deformation of the tube was mainly localized beneath the indentor—the top wall of the tube got pushed in and the opposite wall flattened. Along the tube, the cross-sectional change was not significant. Bending of the (17,0) tube was prominent as the indentor moved by ~18 Å. At this stage the distance between the opposite walls of the tube beneath the indentor was little less than 3 Å. On further loading, flattening progressed along the tube and the distance between the opposite walls below the indentor decreased to ~2 Å. As the indentor radius is larger than the tube radius, the middle portion of the tube became fully flattened and appeared as two graphite sheets separated by ~2 Å. Finally the (17,0) tube failed at a load of ~150 nN and a global strain of 16.4%, which is much smaller than the maximum strain, 40%, of the same tube under uniaxial tension.[2] This clearly indicates that the deformation capacity of a CNT varies with the type of loading.

As stated in the previous section, here again the stiffness of the tube is low due to the large tube length, but as the contact between the tube and indentor is large, asymmetric deformation of the tube does not occur until its breakage at the end. The force-deflection curves of the short and long (34,0) nanotubes are compared in Figure 8. This clearly shows that the load at a particular strain is low for a long tube and the maximum load that the tube can withstand is

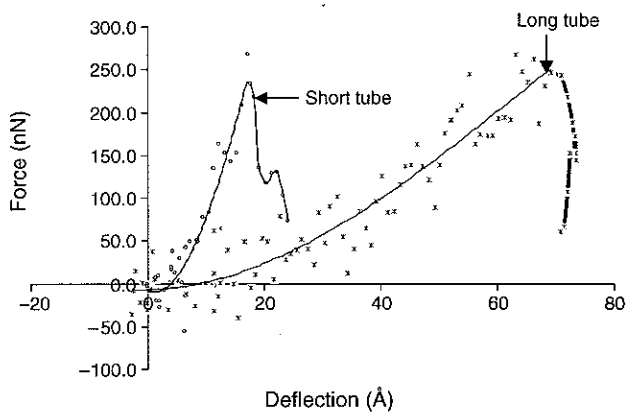

Fig. 8. Force-Deflection curves of (34,0) CNTs of different lengths on loading with the large indentor.

~246 nN, nearly the same, irrespective of the length. The deflection, δ is always larger compared to that for a short tube. This is easily understood assuming that the deflected tube forms a triangle with the original configuration.

4. CONCLUSIONS

This work elucidates the behaviour of CNTs under central loading with an indentor that leads to large deformation and bending. At the same bending angle, the deformation pattern along the tube differs from that of a nanotube under pure bending. It was found that under indentation loading (i) the maximum load that a tube can withstand increases with the tube radii, but is independent of the tube length, and (ii) the maximum bending angle and the maximum global strain are 62° and 14.5% respectively and they are independent of the tube radii. It was also found that the maximum failure strain of a CNT at bending is much smaller than that at uniaxial tension. It was also found that there exists a strong similarity of a CNT bending to a continuum tube bending.

Acknowledgments: The authors thank the Australian Research Council for its continuous financial support. This work was also supported by the Australian partnership for advanced computing.

References

1. B. I. Yakobson, M. P. Campbell, C. J. Brabec, and J. Bernholc, *Comp. Mat. Sci.* 8, 341 (**1997**).
2. K. Mylvaganam and L. C. Zhang, *Carbon* 42, 2025 (**2004**).
3. D. Srivastava, M. Menon, and K. Cho, *Phys. Rev. Lett.* 83, 2973 (**1999**).
4. T. Ozaki, Y. Iwasa, and T. Mitani, *Phys. Rev. Lett.* 84, 1712 (**2000**).
5. D. Srivastava, D. W. Brenner, J. D. Schall, K. D. Ausman, M. Yu, and R. S. Ruoff, *J. Phys. Chem. B* 103, 4330 (**1999**).
6. T. Vodenitcharova and L. C. Zhang, *Phys. Rev. B* 69, 115410 (**2004**).
7. B. I. Yakobson, C. J. Brabec, and J. Bernhole, *J. Comp.-Aided Mater. Design* 3, 173 (**1996**).
8. Y.-S. Zoo, J.-W. An, D.-P. Lim, and D.-S. Lim, *Tribology Letters* 16, 305 (**2004**).
9. M. B. Nardelli and J. Bernholc, *Phys. Rev. B* 60, R16338 (**1999**).
10. W. Shen, B. Jiang, B. S. Han, and S.-S. Xie, *Phys. Rev. Lett.* 84, 3634 (**2000**).
11. T. W. Tombler, C. Zhou, L. Alexseyev, J. Kong, H. Dal, L. Liu, C. S. Jayanthi, M. Tang, and S.-Y. Wu, *Nature* 405, 769 (**2000**).
12. D. W. Brenner, *Phys. Rev. B* 42, 9458 (**1990**).
13. D. W. Brenner, O. A. Shenderova, J. Harrison, S. J. Stuart, B. Ni, and S. B. Sinnott, *J Phys.: Condensed Matter* 14, 783 (**2002**).
14. A. Garg and S. B. Sinnott, *Phys. Rev. B* 60, 13786 (**1999**).
15. L. C. Zhang and H. Tanaka, *Tribology International* 31, 425 (**1998**).
16. L. C. Zhang and H. Tanaka, *JSME International J., Series A: Solid Mechanics and Material Engineering* 42, 546 (**1999**).
17. L. C. Zhang and H. Tanaka, *Wear* 211, 44 (**1997**).
18. L. C. Zhang and T. X. Yu, *Int. J. Pressure Vessels and Piping* 30, 77 (**1987**).
19. T. X. Yu and L. C. Zhang, *Plastic Bending: Theory and Applications*, World Scientific, Singapore (**1996**).
20. T. Vodenitcharova and L. C. Zhang, *Phys. Rev. B* 68, 165401 (**2003**).

Received: 1 November 2004. Accepted: 23 November 2004.